Constructing the Universe with Clusters of Galaxies, IAP 2000 meeting, Paris (France) July 2000
Florence Durret & Daniel Gerbal eds.

DETECTING THE GRAVITATIONAL REDSHIFT OF CLUSTER GAS

Evan Scannapieco and Tom Broadhurst
Department of Astronomy, University of California, Berkeley, CA 94720
European Southern Observatory, Munich, Germany

We examine the gravitational redshift of radiation emitted from within the potential of a cluster. Spectral lines from the intracluster medium (ICM) are redshifted in proportion to the emission-weighted mean potential along the line of sight, amounting to ≈ 50 km/s at a radius of 100 kpc/h, for a cluster dispersion of 1200 km/s. We show that the relative redshifts of different ionization states of metals in the ICM provide a unique probe of the three-dimensional matter distribution. Note that in general gravitational redshifts cause a small overestimate of the recessional velocities of clusters by an average of ~ 20 km/s.

1 Introduction

Recent N-body work has revealed that the central mass profile of cluster-sized dark matter halos in pure Cold Dark Matter (CDM) simulations are relatively flat inside a radius of of ~ 400 kpc, asymptoting to r^{-1} and first described by Navarro, Frenk, and White (NFW).[1] This prediction, although distinct, is not easily examined with lensing observations. The distortion of images by lensing is a powerful way of locating dark matter but is insensitive to the gradient of the distribution, particularly in the central region which is subject to a degeneracy [2,3] Thus the flattening of the slope to r^{-1} cannot be distinguished in practice from a singular isothermal profile from lensing distortions alone (see e.g. Clowe et al.[4]). In principle, the magnifications of lensed sources are more sensitive to the projected mass profile, but their use requires knowledge of both the source redshifts and intrinsic unlensed properties to be reliable.[5,6] Of course all lensing signals relate only to the projected mass distribution and thus provide only indirect information along the line of sight.

Here we describe a means of exploring the distribution of matter in clusters that complements and extends the information available from lensing. This technique is discussed in more detail by Broadhurst and Scannapieco.[7] The gravitational potential of a cluster not only deflects light passing nearby, but imprints a gravitational redshift on light emitted by the cluster itself. The many X-ray emission lines in the metal-rich intracluster medium provide a suitable tracer of this redshift. Since the line emission is generated by a two body process, the velocity information is

weighted by the square of the gas density along a given sight-line, and is quite sensitive to the mass profile in the central region of the cluster. Furthermore, temperature gradients in the gas cause different lines to be emitted at different distances along a line of sight through the cluster, and may thus provide a three-dimensional probe of the matter profile.

While X-ray spectroscopy has been difficult in the past, it is advancing to the point now where this effect may be marginally detected. In the near future, an order of magnitude increase in resolution and effective collecting area will be achieved with improved techniques.

2 Gravitational Redshift

2.1 Simple Analytical Model

The simplest useful model of a cluster is an isothermal sphere in which the density $n(r)$ is proportional to r^{-2} for radii less than a truncation radius R_0, and $n(r) = 0$ for $r > R_0$, so that the gravitational potential is given by

$$\phi(r) = \begin{cases} 2\sigma^2[\ln(r/R_0) - 1] & r < R_0 \\ -2\sigma^2 R_0/r & r > R_0, \end{cases} \tag{1}$$

where σ is the velocity dispersion. The gravitational redshift of light from point sources such as galaxies located within the potential is given simply by

$$\Delta\nu(r) = \nu_0 \frac{\phi(r)}{c^2}, \tag{2}$$

where ν_0 is the rest-frame emission frequency. Spectral line emission from the gas, however, is proportional to $n_e(r) n_{\rm ion}(r)$ and hence assuming the metals are distributed like the electrons we may simply weight the potential by $n^2(r)$ along lines of sight to compute the average redshift. In this case, the frequency of the emission line will be shifted by an amount

$$\Delta\nu(x) = \frac{\nu_0}{c^2} \frac{\int_0^{R(x)} dl\, \phi((x^2+l^2)^{1/2}))n((x^2+l^2)^{1/2})^2}{\int_0^{R(x)} dl\, n((x^2+l^2)^{1/2})^2}, \tag{3}$$

where l is the distance along the line of sight and $R(x) \equiv \sqrt{R_0^2 - x^2}$.

For a singular isothermal sphere then,

$$\begin{aligned} z(x) &= -\frac{\Delta\nu(x)}{\nu_0} = \frac{2\sigma^2}{c^2}\left[\frac{1}{2} - \frac{L(\theta_x) - \theta_x + \theta_x \ln\cos\theta_x}{\theta_x + \sin\theta_x \cos\theta_x}\right] \\ &\approx \frac{2\sigma^2}{c^2}\left[\frac{3}{2} - \ln\left(\frac{2x}{R_0}\right)\right], \end{aligned} \tag{4}$$

where $\theta_x \equiv \arccos(x/R_0)$, $L(\theta_x) \equiv -\int_0^{\theta_x} d\theta \ln(\cos\theta)$ is Lobachevskiy's function, and the approximation is valid for small impact parameters. The velocity dispersion is only a weak function of cosmology [8] and can be estimated as $\sigma = 730\, M_{14}^{1/3}(1+z_c)^{1/2}$ km/s, where M_{14} is the mass of the collapsed halo in units of $10^{14}h^{-1}$ solar masses and z_c is the redshift of collapse. Finally, the relation between the total mass and the velocity dispersion ($\frac{GM}{R_0} = 2\sigma^2$) gives us the truncation radius $R_0 = 400\, M_{14}^{1/3}(1+z_c)^{-1}$ kpc/h.

In the top panel of Figure 1, we plot the redshift as a function of radius for three clusters with $M_{14} = 1.5$, 3, and 6, and $z_c = 0.5$. Here we see that while the gravitational redshift of emission lines near the edge of the cluster is quite small, the r^{-4} weighting boosts the effect significantly along lines of sight near the center of the cluster, reaching $\sim 10\%$ of the velocity dispersion within the inner 10 to 50 kpc.

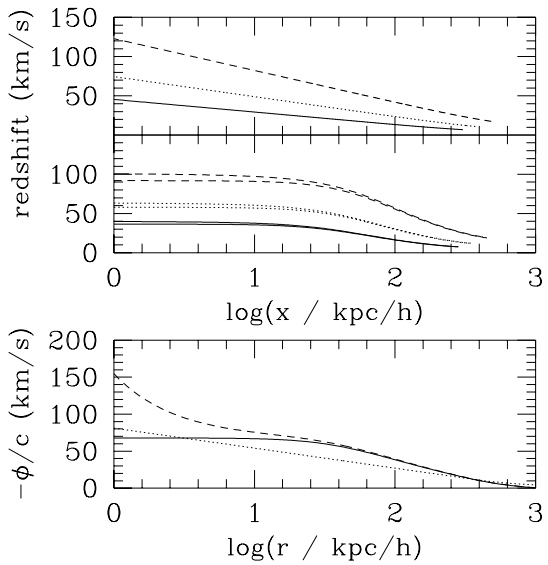

Figure 1: *Top:* Redshift as a function of impact parameter for a singular isothermal profile with $M_{14} = 1.5$, $\sigma = 1000$ (solid), $M_{14} = 3$, $\sigma = 1300$ (dotted), $M_{14} = 6$, $\sigma = 1600$ (dashed). *Center:* Redshift as a function of impact parameter for a nonsingular isothermal profile with masses and velocity dispersions as in the upper panel. In each pair of lines the lower line represents the redshift purely from the profile, while the upper line includes an additional contribution from a cD galaxy modeled as a point mass with 2% of the cluster mass. *Bottom:* Gravitational potential for three different density profiles. The solid lines represent the nonsingular isothermal sphere, the dotted lines show the singular isothermal model, and the dashed lines show a nonsingular model in which a cD galaxy has been added. In all cases $M_{14} = 3$, $\sigma = 1300$, and $z_c = 0.5$ (see §2.1).

2.2 Simple Numerical Model

To better treat the interesting core region of the cluster, let us consider a simple nonsingular model[9] derived by numerically integrating the equation of hydrostatic support of an isothermal gas

$$\frac{d}{d\tilde{r}}\left(\tilde{r}^2 \frac{d\ln\tilde{\rho}}{d\tilde{r}}\right) = -9\tilde{r}^2\tilde{\rho}, \tag{5}$$

where the density and radius have been rescaled such that $\tilde{\rho} \equiv \rho/\rho_0$ and $\tilde{r} \equiv r/r_0$, where ρ_0 is the central density of the cluster and r_0 is the King radius, $r_0 \equiv \sqrt{\frac{9\sigma^2}{4\pi G\rho_0}}$. Integrating outwards from the boundary conditions $\tilde{\rho}(0) = 1$ and $\frac{d\tilde{\rho}}{d\tilde{r}} = 0$ determines the density and gravitational potential at all radii, and we truncate the cluster at $10r_0$.

Again we can relate mass and velocity dispersion and solve for r_0 as a function of mass and redshift, which gives $r_0 = 38\, M_{14}^{1/3}(1+z_c)^{-1}$ kpc/h. We then use $\phi(r)$ and $n(r)$ to numerically integrate Eq. 3 to obtain the mean redshift of lines as a function of impact parameter x. In the center panel of Figure 1 we plot our results for three clusters of mass $M_{14} = 1.5$, 3, 6 and $z_c = 0.5$, as the results for a nonsingular sphere in which the potential associated with a central cD galaxy has been simply added to the numerical solution, modeled as a point mass with 2% of the cluster mass. For reference, we also plot $\phi(r)$ for the singular, nonsingular, and nonsingular plus point mass models in the bottom panel.

In this figure we see that the singular and nonsingular isothermal models have much the same $z(x)$ profiles outside the core radius, but the presence of a core creates a sharp turnover at small radii, allowing these two potentials to be easily distinguished. Note also that the sharp increase in $\phi(r)$ at very small radii in the core plus point mass model leads to only a ~ 10 km/s increase in the observed line redshifts, due to averaging along the line of sight.

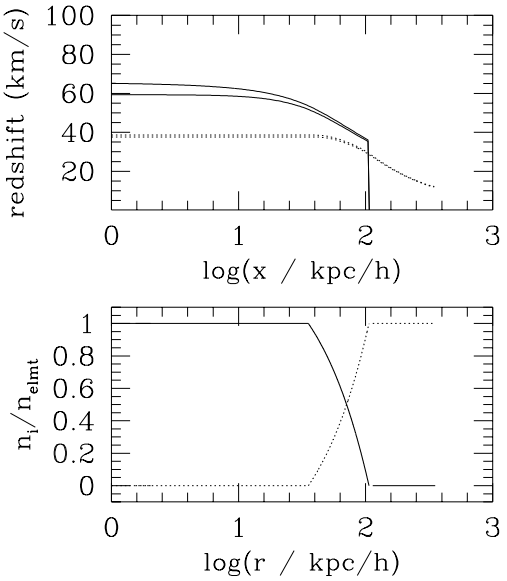

Figure 2: Gravitational redshift for the $M_{14} = 3$ model in Figure 2 in which the effects of temperature variations are modeled simply by taking the fractional ionization between two ionization states to vary linearly from $1r_0$ to $3r_0$. The lower ionization state is given by the solid lines and the higher by the dotted lines. *Top:* Observed gravitational redshift of the lines from the two ions as a function of impact parameter of the line of sight. *Bottom:* The fractional number densities of each ionization state as a function of radial distance.

3 Temperature Gradients

The models adopted in §2 were intended only as illustrative, and by no means represent the full physics of the cluster dark matter and gas. The evolution of the dark matter in clusters is complex, many showing clear evidence for recent mergers.[10,11,12] For many quiescent clusters, however, the radial profile of simulated clusters in CDM models are given by a universal density profile as shown in NFW. Unlike the simple models considered in §2, however, the redshift estimate provided by Eq. 3 does not tell the full story for this model, as it does not account for the presence of a temperature gradient.

In general the gravitational redshift will not only be a function of gas density along the line of sight, but of the temperature profile as well. The ionization potential of each emission line will be strongly peaked about its ionization temperature (e.g. Zombeck [13]), and hence an emitted line will be confined to within a hollow shell in the cluster. Thus, with measurements of different X-ray emission lines, one can hope to simultaneously solve for the potential and the temperature profile, gaining three-dimensional information. This must be taken into account in a NFW potential and will be especially important for clusters containing cooling flows. In this case the temperature gradient may exceed two orders of magnitude, so that for example the excitation of iron may range from FeX to FeXXVI.[14,15]

A simple illustration of the additional information afforded by temperature variations is given in Figure 2. Here the fractional ionization between two ionization states X_{i+1} and X_i is allowed to vary linearly from $1r_0$ to $3r_0$, in the potential given in §2.2, with $M_{14} = 3$ and both with and without a point mass. We interpret this model as a cooling-flow configuration in which the higher ionization state cannot exist within the core region of the cluster where the temperature drops much lower than its ionization potential. Here we see that the x beyond which X_i is completely ionized to the higher state is marked by an abrupt cutoff in line emission. The x at which X_{i+1} completely recombines to the lower state is marked by a leveling off in the redshift as a function of x, accompanied by a continuing increase in redshift as a function of x

in the lines from the lower ionization state. Along lines of sight such that $r_0 \leq x \leq 3r_0$, which at $\ell = 0$ pass through the partially ionized region, we see that the lines are offset from each other, providing information as to the width of the transition region along the line of sight. This can be compared to the width of the partially ionized region in the x direction to determine the sphericity of the cluster.

4 Future Prospects and Observational Issues

While the systematic redshift of cD galaxies examined above provides a tantalizing suggestion of cluster gravitational redshifts, the possibility of subtle substructure makes studying optical emission from cluster galaxies difficult to apply accurately. At best such studies are limited by the finite number of bright cluster members for measuring accurate velocities.

Thus the X-ray spectroscopic approach outlined in §2 and §3 will provide the most straightforward method for studying gravitational redshifts. Note that this requires both high spectral resolution to determine the shift of the line centroids, and fair spatial resolution to obtain radial information. Little information can be learned from a purely spectral analysis, however, as the overall cluster-integrated line profile is indistinguishable from a thermal profile with a slightly broadened width.

The exploration of this effect may be marginally possible with the current generation of X-ray satellites. The High-Energy Transmission Grating on the Chandra Satellite, launched in July 1999, has a resolving power of $E/\Delta E \approx 2,000 = 600$ km/s in the 1 to 2 keV range,[a] and the Reflection Grating Spectrometer on the XMM satellite launched in December 1999 provides $E/\Delta E$ values from 200 to 800 in the energy range 0.35 to 2.5 keV as described by T. Tamura and M. Arnaud in this volume.[b] Typically, using multiple emission lines, one can achieve resolutions of 10% of these values, suggesting that investigations of gravitational redshifts in rich clusters may be possible but challenging. Note that the thermal velocity of the ions is smaller than σ by a factor of $\sqrt{m_p/m_{\rm ion}}$.

The next generation of satellites will significantly increase these capabilities. The Spectroscopy X-ray Telescope (SXT) on the proposed Constellation X team of X-ray telescopes plans to use both a quantum microcalorimter with 2 eV resolution and a set of reflection gratings below 2 keV, to obtain velocity sensitives better than 100 km/s below 1 keV and of the order of 20 km/s at higher energies.[c] The narrow field detectors on the proposed XEUS observatory in space promise similar resolutions.[d] With such sensitivities, both core-profile studies such as shown in Figure 1 and multiple-line, three-dimensional studies as described in §3 will be well within reach.

Some observational issues are difficult to predict. As line emission is proportional to $n_e(r)n_{\rm ion}(r)$, metallicity gradients can bias gravitational redshift measurements. Such gradients have already been discovered in the Centaurus Cluster [16] and the cluster AWM 7, [17] and will undoubtedly be a subject of investigation for the current generation of X-ray satellites. As in some cases the metallicity can vary by a factor of two over the cluster, these gradients must be well understood before our approach is applied.

Large-scale bulk motion of gas should also be detected from recent group infall in some clusters. The disturbance of the intracluster medium by gas infall has been claimed to be significant over a period of 3 Gyrs in favorable conditions, before shocks are thermalised and bulk flow through the core ceases. [18] If infall is common then the relatively small perturbation to the line centroid by gravity proposed here may be made noisy by the continuous process

[a] http://space.mit.edu/HETG/
[b] http://astro.estec.esa.nl/XMM/user/uhb/xmm_uhb.html
[c] http://constellation.gsfc.nasa.gov/design/resolution.html
[d] http://astro.estec.esa.nl/SA-general/Projects/XEUS/

of cluster interaction, or perhaps in some cases relegated to a correction applied to a larger dynamical disturbance. Finally the relativistic temperatures in the cluster gas will cause a small shift in X-ray line emission by a factor of $\gamma - 1 \approx \frac{kT(r)}{m_{\rm ion}c^2}$ due to relativistic beaming and the transverse Doppler effect, but fortunately this is smaller than the gravitational redshift by a factor of $m_p/m_{\rm ion}$.

These and other issues will await the new and next generations of X-ray telescopes. It is clear, however, that whatever the experimental challenges, a careful measurement of X-ray emission lines over the surface of galaxy clusters will be a useful probe of cluster structure and formation.

Acknowledgments

We wish to thank Yuri Levin, Avi Loeb, Micheal Rauch, and Zofia Rawner for useful input during this investigation and for help in its presentation.

References

1. J. F. Navarro, C.S Frenk, and S. D. M. White, ApJ **490**, 493 (1997)
2. P. Schneider and C. Seitz, A&A **294**, 411 (1995)
3. N. Kaiser, ApJ **439**, L1 (1995)
4. D. Clowe, G. A. Luppino, N. Kaiser, J. P. Henry, and I. M. Gioia, ApJ **497**, L61 (1998)
5. T. Broadhurst, A. N. Taylor, and J. A. Peacock, ApJ **438**, 49 (1995)
6. A. N. Taylor, S. Dye, T. Broadhurst, and N. Benitez, and E. van Kampen, ApJ **501**, 539 (1998)
7. T. Broadhurst & E. Scannapieco ApJ **533**, L93 (2000)
8. V. R. Eke, S. Cole, and C. S. Frenk, MNRAS **282**, 263 (1996)
9. J. Binney and S. Tremaine, *Galactic Dynamics* (Princeton University Press, Princeton, 1987)
10. A. I. Zabludoff and D. Zaritsky, ApJ **447**, 21 (1995)
11. C. M. Bird, D. S. Davis, and T. C. Beers, AJ1099201995
12. N. Bliton, E. Rizza, J. O. Burns, F. N. Owen, and M. J. Ledlow, MNRAS **301**, 609 (1998)
13. M. V. Zombeck, *Handbook of Space Astronomy and Astrophysics*, (University Press, Cambridge, 1990)
14. A. C. Fabian, ARA&A **32**, 277 (1994)
15. E. Churazov, R. Sunyaev, M. Gilganov, W. Forman, and C. Jones, MNRAS **297**, 1279 (1998)
16. Y. Fukazawa, T. Ohashi, A. C. Fabian, C. R. Canizares, Y. Ikebe, K. Makishima, R. F. Mushotzky, and K. Yamashita, PASJ **46**, L55 (1994)
17. H. Ezawa, Y. Fukazawa, K. Makishima, T. Ohashi, F. Takahara, H. Xu, and N. Y. Yamasaki, ApJ **490**, L33 (1997)
18. K. Roettiger, J. O. Burns, and C. Loken, ApJ **473**, 651 (1996)